JAERI-M
87-167

DIVERTOR CHARACTERISTICS IN OHMICALLY AND NEUTRAL-BEAM-HEATED JT-60 DISCHARGES

October 1987

Hiroo NAKAMURA, Toshiro ANDO, Hidetoshi YOSHIDA
Setsuo NIIKURA*, Takeo NISHITANI and Keisuke NAGASHIMA

日 本 原 子 力 研 究 所
Japan Atomic Energy Research Institute

JAERI-Mレポートは，日本原子力研究所が不定期に公刊している研究報告書です。
入手の問合わせは，日本原子力研究所技術情報部情報資料課（〒319-11 茨城県那珂郡東海村）あて，お申しこしください。なお，このほかに財団法人原子力弘済会資料センター（〒319-11 茨城県那珂郡東海村日本原子力研究所内）で複写による実費領布をおこなっております。

JAERI-M reports are issued irregularly.
Inquiries about availability of the reports should be addressed to Information Division Department of Technical Information, Japan Atomic Energy Research Institute, Tokaimura, Naka-gun, Ibaraki-ken 319-11, Japan.

編集兼発行　日本原子力研究所
印　　刷　日青工業株式会社

JAERI-M 87-167

DIVERTOR CHARACTERISTICS IN OHMICALLY AND NEUTRAL-BEAM-HEATED JT-60 DISCHARGES

Hiroo NAKAMURA, Toshiro ANDO+, Hidetoshi YOSHIDA, Setsuo NIIKURA*
Takeo NISHITANI and Keisuke NAGASHIMA

Department of Large Tokamak Research
Naka Fusion Research Establishment
Japan Atomic Energy Research Institute
Naka-machi, Naka-gun, Ibaraki-ken

(Received September 25, 1987)

Divertor characteristics in particle and energy control in neutral-beam (NB) heated discharges on JT-60 have been studied with injection power of up to 20 MW. The essential divertor functions are successfully obtained. In ohmically heated discharges, minimum clearances between the separatrix magnetic surface and the fixed limiter for sufficient divertor action are 1.5 cm at $\bar{n}_e = 1.5 \times 10^{19}$ m^{-3} and 2.5 to 3 cm at $\bar{n}_e = 4 \times 10^{19}$ m^{-3}. Global power balance studies show that, in the NB-heated divertor discharge, about 5% to 10% of the total absorbed power, P_{ABS}, is radiated from the main plasma, while 50% to 60% is radiated in the limiter discharge. At $\bar{n}_e = 6 \times 10^{19}$ m^{-3}, 50% of P_{ABS} flows to the divertor plate. The radiation loss in the divertor chamber is 15% of P_{ABS}. According to the spatial distribution of the temperature rise on the divertor plate, the half width of the heat load is less than 1 cm at $\bar{n}_e = 1.5$ to 4.4×10^{19} m^{-3}. Neutral pressures in the divertor chamber and around the main plasma increase in proportion to $\bar{n}_e^2$. Compression ratio is about 45. The effectiveness of the divertor pumping system in particle control is shown for

---

+ Department of JT-60 Facility

* On leave from Mitsubishi Atomic Power Industries, Inc.

NB-pulses of at least 1 second. Reduction of evaporation by separatrix swing is also shown.

Keywords: JT-60, Divertor, Particle Control, Energy Control, Neutral Pressure, Compression Ratio, Particle Exhaust, Power Balance, Remote Cooling, Separatrix Swing

ＪＴ－60のジュール加熱および中性粒子入射加熱実験におけるダイバータ特性

日本原子力研究所那珂研究所臨界プラズマ研究部
中村　博雄・安東　俊郎＋・吉田　英俊・新倉　節夫＊
西谷　健夫・永島　圭介

（ 1987年9月25日受理 ）

1986年3月から11月までの，ＪＴ－60のジュール加熱（OH）および中性粒子加熱入射（NBI）加熱実験におけるダイバータ特性について述べた。主プラズマ回り中性粒子圧力（P_{H2}^{MAIN}）およびダイバータ室中性粒子圧力（P_{H2}^{DIV}）は，OHおよびNBI実験ともに，主プラズマ電子密度$\bar{n}_e$の2乗に比例して増加し，圧縮比（$= P_{H2}^{DIV} / P_{H2}^{MAIN}$）は45である。NBI実験での粒子排気特性では，$\bar{n}_e$が$6 \times 10^{19}\ m^{-3}$以下の時，ダイバータ板による粒子排気が主であるのに対し，$6 \times 10^{19}\ m^{-3}$以上では，ダイバータ排気装置による粒子排気が主である事が明らかになった。また，ダイバータ板近傍での熱負荷の半値幅は，1cm以下である。NBI実験でのパワーバランス測定によれば，主プラズマ輻射損失は全吸収パワーの5～10％である。また，ダイバータ室での輻射損失は15％，ダイバータ板への熱負荷は50％である。ヘリウムガスを使用したNBI実験（$H^0 \rightarrow He$）中に，Moによる輻射損失の急増が見られたが，セパラトリクス磁気面をダイバータ板上で振動させることにより抑制出来た。以上の結果，20MWのNBI加熱実験においても，粒子・不純物および熱負荷が十分制御可能であることが明らかになった。

那珂研究所：〒311－02　茨城県那珂郡那珂町大字向山801－1
＋　ＪＴ－60試験部
＊　外来研究員　三菱原子力工業㈱

CONTENTS

目　　次

1. INTRODUCTION

To achieve a reactor-grade plasma, impurity, energy, and particle control by divertor is essential. At first, successful divertor actions on these items have been demonstrated for ohmically heated (OH) discharges in a small tokamak DIVA[1]. Following DIVA, divertor studies for OH and neutral beam (NB) heated discharges with heating powers of up to 7 MW have been performed extensively in medium size tokamaks such as ASDEX[2,3], DIII[4] and PDX[5]. The high confinement discharge (H-mode) was discovered in NB heated ASDEX discharges[6]. In the DIII with an open divertor, reduction of heat load to the divertor plate by high recycling was discovered for the OH discharges[7-9] and also for the NB heated ones. In these tokamaks, successful impurity control has been shown. The open divertor experiment in JFT-2M has also been reported[10]. These results show the attractiveness of the poloidal divertor. However, to apply a poloidal divertor concept to a reactor-grade device, the above divertor characteristics have to be studied in large-size tokamaks. Recently, two large tokamak experiments, DIII-D[11] and JET[12], have reported H-mode discharges with NB injection of up to 10 MW.

JT-60 is a large tokamak device (R = 3 m, a = 0.93 m, B_t = 4.5 T, I_p = 2.7 MA) with a single null poloidal divertor in the midplane at the torus outside[13,14]. In JT-60, the divertor characteristics have been studied in detail. Experimental results for the OH discharges from April 1985 to March 1986 are described elsewhere[15-17]. In these OH discharges, the divertor actions similar to those in the above tokamaks were observed. Experimental results for the NB heated discharges from July to November 1986 with NB power of up to 20 MW are also described elsewhere[19,20]. In this paper, the details of the divertor characteristics in these experiments are presented.

In the following section, experimental arrangements are described. In Section 3, the experimental results on particle and energy control are discussed. Section 4 gives the discussion of the divertor characteristics. Section 5 provides summary.

2. EXPERIMENTAL ARRANGEMENTS

Details of the JT-60 device are described in Ref. [21]. The inner surfaces of the vacuum vessel are fully covered by armor plates, fixed toroidal limiters, and divertor plates[22], made of TiC-coated Mo and Inconel 625[23]. Plane view of diagnostics and major components are shown in Fig. 1. The major diagnostics used for the following study are shown in Fig. 2. There are a total of 18 port sections. Neutral pressure in the divertor chamber is measured by a fast ionization gauge in the upper divertor chamber at the No. 13 port section (P-13). Total time delay is about 100 ms. Neutral pressure around the main plasma is measured by a standard ionization gauge at the P-10 section. Total time delay is about 250 ms. Radiation loss and H_α intensity are measured in the divertor chamber for upper and lower divertors, respectively. Heat load to the divertor plate is measured by 6-channel brazed thermocouples for the upper and lower divertors at the P-1 section. Radiation loss and H_α intensity around the main plasma are measured by 4-channel (3-channel vertical; 1-channel near X point) detectors. Moreover, 15-channel bolometers and 4-channel H_α photodiodes viewing the inner wall are used. To control backflow and recycling of neutrals from the divertor chamber, there are four divertor pumping systems[24]. These systems are composed of Zr/Al getter pumps with a total effective pumping speed of about 6.8 m^3/s for hydrogen at 20°C. Moreover, to improve divertor pumping capability of the torus vacuum pump, additional plates are attached at the inlet of the vacuum pumping port. In the divertor operation, the clearance between the separatrix magnetic surface and fixed toroidal limiter was changed from 0.2 to 5.1 cm. Also, the clearance between the separatrix magnetic surface and the armor attached to a main magnetic limiter coil is changed from 1 to 9 cm.

3. EXPERIMENTAL RESUTLS

Waveforms from a typical NB-heated hydrogen divertor discharge with I_p = 2 MA and P_{NBI}=13.4 MW are shown in Fig. 3. In this figure, a density reduction during the NB injection heating is observed. Also, observed are increases of neutral pressures around the main plsama and

2. EXPERIMENTAL ARRANGEMENTS

Details of the JT-60 device are described in Ref. [21]. The inner surfaces of the vacuum vessel are fully covered by armor plates, fixed toroidal limiters, and divertor plates[22], made of TiC-coated Mo and Inconel 625[23]. Plane view of diagnostics and major components are shown in Fig. 1. The major diagnostics used for the following study are shown in Fig. 2. There are a total of 18 port sections. Neutral pressure in the divertor chamber is measured by a fast ionization gauge in the upper divertor chamber at the No. 13 port section (P-13). Total time delay is about 100 ms. Neutral pressure around the main plasma is measured by a standard ionization gauge at the P-10 section. Total time delay is about 250 ms. Radiation loss and H_α intensity are measured in the divertor chamber for upper and lower divertors, respectively. Heat load to the divertor plate is measured by 6-channel brazed thermocouples for the upper and lower divertors at the P-1 section. Radiation loss and H_α intensity around the main plasma are measured by 4-channel (3-channel vertical; 1-channel near X point) detectors. Moreover, 15-channel bolometers and 4-channel H_α photodiodes viewing the inner wall are used. To control backflow and recycling of neutrals from the divertor chamber, there are four divertor pumping systems[24]. These systems are composed of Zr/Al getter pumps with a total effective pumping speed of about 6.8 m^3/s for hydrogen at 20°C. Moreover, to improve divertor pumping capability of the torus vacuum pump, additional plates are attached at the inlet of the vacuum pumping port. In the divertor operation, the clearance between the separatrix magnetic surface and fixed toroidal limiter was changed from 0.2 to 5.1 cm. Also, the clearance between the separatrix magnetic surface and the armor attached to a main magnetic limiter coil is changed from 1 to 9 cm.

3. EXPERIMENTAL RESUTLS

Waveforms from a typical NB-heated hydrogen divertor discharge with I_p = 2 MA and P_{NBI}=13.4 MW are shown in Fig. 3. In this figure, a density reduction during the NB injection heating is observed. Also, observed are increases of neutral pressures around the main plsama and

in the divertor chamber. A significant increase of the radiation loss in the divertor chamber and the temperature rise in the divertor plate is also noted.

3.1 PARTICLE CONTROL

3.1.1 NEUTRAL PRESSURE BUILD-UP

In Fig. 4, strong nonlinear dependence of neutral pressures in the divertor chamber ($P_{H_2}^{DIV}$) and around the main plasma ($P_{H_2}^{MAIN}$) on the main plasma density ($\bar{n}_e$) are shown in the OH and NB heated discharges. $P_{H_2}^{DIV}$ and $P_{H_2}^{MAIN}$ increase approximately in proportion to $\bar{n}_e^2$, the same results as observed in ASDEX[4] and DIII[10]. Maximum pressures in this experiment are 0.63 Pa for $P_{H_2}^{DIV}$ and 0.014 Pa for $P_{H_2}^{MAIN}$ at $\bar{n}_e = 7.2 \times 10^{19}$ m^{-3} with $I_p = 2$ MA and $P_{NBI} = 20$ MW. To study the effect of gas injection location on plasma properties, two types of gas injection experiments have been done. In the characteristics of the neutral pressure buildup ($P_{H_2}^{DIV}$, $P_{H_2}^{MAIN}$), there is no clear difference between the main plasma gas injection experiment and the divertor chamber gas injection one. However, the rate of density increase in the divertor gas injection case is higher than that in the main plasma gas injection case. Above the plasma density of 4×10^{19} m^{-3}, there is a small dependence of $P_{H_2}^{DIV}$ and $P_{H_2}^{MAIN}$ on plasma current. The neutral pressures in discharges with $I_p = 1.5$ MA are higher than the ones with $I_p = 2$ MA. This difference is considered to be caused by the I_p dependence of the global particle confinement time τ_p (small I_p gives small τ_p). Therefore, influx to the divertor chamber (N_e/τ_p) depends on I_p.

3.1.2 COMPRESSION RATIO

Compression ratio C is defined as the ratio of the pressure in the divertor chamber, $P_{H_2}^{DIV}$, to the pressure in the main plasma, $P_{H_2}^{MAIN}$ and can be calculated by the following equation;

$$(P_{H_2}^{DIV} - P_{H_2}^{MAIN})C = R \cdot N_e/\tau_p$$

Figure 5 shows the relationship between $P_{H_2}^{DIV}$ and $P_{H_2}^{MAIN}$ in the range of $\bar{n}_e = 1.5\text{~}9.1\times10^{19}$ m^{-3}. The compression ratio is around 45 for both OH

and NB heated discharges. The compression ratio in the divertor chamber gas injection case is almost the same as that in the main plasma gas injection case in JT-60, although in ohmically heated PDX experiment[25] the compression ratio in the divertor chamber gas injection case was twice as high as that in the main plasma gas injection case. Since the compression ratio is almost constant, the conductance betwen the main plasma and the divertor chamber is expected to be constant. The conductance is calculated to be about 900 m^3 from $RN_e/(\tau_p P_{H_2}^{DIV})$(because $P_{H_2}^{DIV} >> P_{H_2}^{MAIN}$) where N_e is the total number of electrons in the main plasma and R is the recycling ratio. This value is about 1/2 to 1/3 of the calculated mechanical conductance at the divertor throat. This reduction of the conductance appears to be qualitatively reasonable because the scrape-off plasma reduces the back flow to the main plasma. From the constant conductance and the $\bar{n}_e$ dependence of τ_p ($\propto \bar{n}_e$-1) [26,27], the τ_p degradation factor becomes proportion to $\bar{n}_e^2/P_{H_2}^{DIV}$. Figure 6 shows the dependence of $\bar{n}_e^2/P_{H_2}^{DIV}$ on the absorbed power P_{ABS}. The 2 MA data shows a higher value of $\bar{n}_e^2/P_{H_2}^{DIV}$ than the 1.5 MA data. This dependence is similar to that of the energy confinement time. This resemblance suggests a correlation between the particle and energy confinement[19].

3.1.3 PARTICLE EXHAUST

Total particle exhaust rate N_e/τ_p^* is given by the following equation:

$$N_e/\tau_p^* = Q_{exhaust} + Q_S \quad ,$$

where τ_p^* is the effective particle confinement time [$=\tau_p/(1-R)$], $Q_{exhaust}$ is the exhaust rate by the divertor pumping system, and Q_s by the TiC-coated Mo plate. Particle exhaust rate $Q_{exhaust}$ is divided into $Q_{Zr/Al}$ and Q_V, where $Q_{Zr/Al}$ is the exhaust rate by the Zr/Al getter pump systems and Q_V by the torus vacuum pumping systems. Using pressures and pumping speeds of each system, $Q_{Zr/Al}$ and Q_V are given by 5.3 $P_{H_2}^{DIV}$ and 40 $P_{H_2}^{DIV}$ (Pa·m^3/s), where $P_{H_2}^V$ is the neutral pressure in the manifold of the torus vacuum pumping system. Since the ratio of $Q_{Zr/Al}$ to Q_V is about 3, $Q_{exhaust}$ can be given by 6.8 $P_{H_2}^{DIV}$. Density dependence of $Q_{exhaust}$ can also be seen from Fig. 4. The ratio of

$Q_{Zr/Al}$ to Q_V is about 3. $Q_{exhaust}$ increases approximately in proportion to $\bar{n}_e^2$. At $\bar{n}_e = 6\times10^{19}$ m^{-3}, $Q_{exhaust}$ is 3 Pa m^3/s, which is as large as the fueling rate by the neutral beam injection of 20 MW with a beam energy of 75 keV. This shows that long-pulse NB injection was made possible by the divertor pumping system. The particle exhaust rate by the TiC surface, Q_S, is calculated by $(N_e/\tau_p^*) - Q_{exhaust}$. Since almost all ion fluxes are guided into the divertor chamber, the pumping rate of first wall Q_S is assumed to be equal to that of the divertor plate Q_{DIV}. Figure 7 shows the density dependence of N_e/τ_p^*, $Q_{exhaust}$, and Q_V in the NB-heating experiment. In this calculation, τ_p^* is 0.7 s for P_{ABS} > 13 MW [27]. N_e/τ_p^* increases linearly with $\bar{n}_e$. On the other hand, $Q_{exhaust}$ increases in proportion to $\bar{n}_e^2$. The calculated value of Q_{DIV} increases up to $\bar{n}_e$= 5 to 6×10^{19} m^{-3}. But above that density, Q_{DIV} saturates gradually at 3 Pa·m^3/s. Q_{DIV} in a fresh surface of the divertor plate was obtained in limiter-divertor transition experiment. Wave form of $\bar{n}_e$ is shown in Fig. 8. At t=4.1 sec, $\bar{n}_e$ decreases drastically. If this reduction is assumed to be caused by surface pumping of a fresh divertor plate, Q_{DIV} is estimated to be 8.3 Pa·m^3/s for τ_p=90 ms. At $\bar{n}_e = 6\times10^{19}$ m^{-3}, N_e/τ_p^*, $Q_{exhaust}$, and Q_{DIV} are 6.0, 3.0, and 3.0 Pa·m^3/s, respectively. Below $\bar{n}_e = 6\times10^{19}$ m^{-3}, the particle balance is dominated by the surface pumping capacity of the divertor plate. Above that density, the exhaust rate of the divertor pumping system becomes dominant. Saturation tendency of the divertor plate is shown in Fig. 9. In this experiment, $\bar{n}_e$ feedback control was started at t=4 sec. During a flat-top plase of $\bar{n}_e$, fueling rate of injection gas Q_c decreases gradually. This decrease is expected to be caused by saturation characteristics of the divertor plate.

Typical results of density control in the NB-heating experiment are shown in Fig. 10 for the limiter discharge and Fig. 11 for the divertor discharge. To control density in the case of the limiter discharge, additional pumping systems with large pumping speed are necessary. In the case of the divertor discharge, the density is easily controlled by changing the gas puffing rate even in the high-density condition (6×10^{19} m^{-3}).

3.1.4 SCRAPE-OFF THICKNESS FOR DIVERTOR ACTION

In order to keep the efficient influx into the divertor chamber and to suppress the plasma wall interaction, the clearance between the separatrix magnetic surface and the fixed limiter must be sufficienlty wide. On the other hand, considering the plasma-shaping coil current capability, the maximum distance cannot be arbitrarily large. So, to clarify the minimum clearance, dependence of H_α intensity, neutral pressure, and radiation loss in the divertor chamber on the clearance was studied by changing the clearance during the ohmically-heated discharge. Figures 11 and 12 show results of these dependences for the H_α intensity, the neutral pressure and the radiation loss, respectively. These results show that the minimum clearances are 1.5 cm at $\bar{n}_e=1.5\times10^{19}$ m^{-3} and 2.5 to 3 cm at $\bar{n}_e=4.0\times10^{19}$ m^{-3}.

In the NB-heated discharge, a detailed experiment similar to the ohmically-heated discharge was not performed. However, comparing a shot with 2 cm of clearance and one with 4 cm of clearance, the neutral pressures in the divertor chamber are almost the same. In these cases, the mean plasma density is around 2 to 4×10^{19} m^{-3}. Therefore, the minimum clearance in the NB-heated discharge is expected to be less than 2 cm. However, to clarify this dependence more clearly, further study is necessary.

3.2 ENERGY CONTROL

3.2.1 GLOBAL POWER BALANCE

Global power balance for a 2 MA NB heated discharge is shown in Fig. 14. P_{ABS} means the net absorbed power in the main plasma ($=P_{NB}+P_{OH}-P_{SHINETHROUGH}$). P_{RAD}^{DIV} and P_{RAD}^{MAIN} are radiation losses in the divertor chamber and the main plasma, respectivley. $P_{T/C}^{DIV}$ is the heat load which is deposited on the divertor plate. This figure shows that a major fraction of the absorbed power is exhausted to the divertor chamber. With the increase of $\bar{n}_e$, reduction of the heat load on the divertor plate is observed, the same tendency as observed in ASDEX[2] and DIII[8]. At $\bar{n}_e=6\times10^{19}$ m^{-3}, $P_{T/C}^{DIV}$ is about 50% of P_{ABS} in the range of $\bar{n}_e=1.5$ to 7.3×10^{19} m^{-3}. Total radiation loss from the divertor

chamber (P_{RAD}^{DIV}) is about 15% of P_{ABS}. Dependence of P_{RAD}^{DIV} in ion and electron sides on $\bar{n}_e$ is discussed in later part of this section on Fig. 19.

Two causes for the missing power in the global power balance are considered. One is the radiation loss from the divertor chamber outside the field of view of the bolometers. In the estimation of the divertor radiation loss, one channel looking at the separatrix on the divertor plate is used for the upper and lower divertor, respectively. Another channel looking at the divertor plate near the divertor throat showed almost the same intensity as the above channel in the high-density case. Another cause of the missing power is the radiation loss in the region near the X-point. In this region, a significant increase of the bolometer signal with $\bar{n}_e$ was observed. Therefore, these two radiation losses are considered to be the main causes of the missing power and the fraction of remote radiative cooling in the divertor chamber is considered to be larger than the value shown in Fig. 14.

The effectiveness of the divertor on the impurity control is shown in Fig. 15. In limiter discharges, the ratio of radiation losses in the main plasma to the absorbed power, P_{RAD}^{MAIN}/P_{ABS}, is in the range of 50% to 60%. In the divertor discharges, on the other hand, a significant reduction of these ratios is observed. In the NB-heating discharges, this ratio is in the range of 5% to 10%.

3.2.2 RADIATION LOSS IN DIVERTOR CHAMBER

Radiation losses in the divertor chamber, P_{RAD}^{DIV}, are shown in Fig. 16 for the OH discharges and Fig. 17 for the NB-heated discharges. In the OH case, P_{RAD}^{DIV} increases non-linearlly with $\bar{n}_e$. But, P_{RAD}^{DIV} becomes saturated and decreased above $\bar{n}_e = 3\text{-}4\times10^{19}$ m^{-3}. This tendency is considered to be caused by reduction of divertor plasma temperature ($T_e < 10$ eV). Computor simulation result by the divertor code show similar $\bar{n}_e$ dependence to the experimental data, while the measured P_{RAD}^{DIV} is by a factor of two to three greator than the simulation result[28]. Since the simulation includes only hydrogen line radiation, this difference between the simulation and the experimental results can be explained by impurity line radiation, and so on. For example, the radiation loss with the oxygen contents of 1.25% is same as these difference. P_{RAD}^{DIV} in the NB-heating phase is about ten times larger

than in the ohmic heating phase. R_{RAD}^{DIV} on the ion drift side is larger than on the electron drift side. On the ion side, P_{RAD}^{DIV} increases nonlinearly with $\bar{n}_e$, but P_{RAD}^{DIV} saturates and decreases above $\bar{n}_e$=3 to 4×10^{19} m^{-3}. This tendency is considered to be caused by a reduction of the divertor plasma temperature. On the other hand, on the electron side, P_{RAD}^{DIV} increases with $\bar{n}_e$. Although the cause of these asymmetries is not clear, the effect of fast ions is considered to be one of the cause.

3.2.3 HEAT LOAD ON DIVERTOR PLATE

Energy deposition on the divertor plate is measured by an array of brazed-thermocouples. Typical time response is shown in Fig. 3. Spatial distributions of the temperature rises, ΔT, in the upper (ion drift side) and lower (electron drift side) divertor plates are shown in Fig. 19 for the low-density case ($\bar{n}_e=1.5\times10^{19}$ m^{-3}) and in Fig. 18 for the high-density case ($\bar{n}_e=4.4\times10^{19}$ m^{-3}). In both cases, duration of the NB pulse is 0.5 s. Due to separation between thermocouple location and heat flux peak and time response of the thermocouples, maximum temperature rises are observed at t = 7.5 s, while the NB-pulse was terminated at t = 7.0 s. In the low-density case, the temperature rises in the electron drift and ion drift sides are almost the same. In the high-density case, the temperature rise in the ion drift side is higher than the rise in the electron side. Moreover, the total heat load on the divertor plate on the ion side was about two times that on the electron side. In both cases, half widths of the temperature rise in the ion and the electron drift sides are less than the thermocouple separation of 2 cm. Since the angle between the divertor plate and the separatrix line is about 30 deg, the half width of the heat flux in front of the divertor plates is less than 1 cm. In this experiment, density dependence of the half width on the heat flux is not clear because the interval of the thermocouple is 2 cm. In the NB-heated discharges, time-averaged heat load in the NB-heating phase has been calculated from the equilibrium temperature distribution at 30 s after the discharge. In this calculation, thermal radiation from the divertor plate is neglected. First, the time-averaged heat load in the NB-heated discharge, Q_{OH+NB}(MJ), is calculated. Next, the heat load in the ohmic discharge with the same I_p and $\bar{n}_e$, Q_{OH}, is calculated. Q_{NB}

is then given by $Q_{OH+NB} - Q_{OH}$. As a result, the ratio of the total heat load deposited on the divertor plate to the absorbed NB power, $Q_{NB}/(P_{ABS}\Delta t_{NB})$, is calculated to be 50% to 70% for $\bar{n}_e$=1.5 to 6×10^{19} m^{-3}. Total heat load on the ion drift side is about two times larger than that on the electron drift side. Assuming a 2 cm heat disposition width in the NB-heating phase, the time- and spatial-averaged heat flux is around 1000 W/cm^2 for a 20 MW injection.

3.2.4 HEAT LOAD REDUCTION BY SEPARATRIX SWING

In the NB-heated hydrogen divertor discharges, molybdenum impurity was not observed up to 20 MW of NB injection power. However, in the case of helium discharges with NB power larger than about 10 MW, a molybdenum burst is observed after 100 to 200 ms from the start of NB heating. According to estimations of the total heat load on the divertor plate, there is not much difference between hydrogen and helium discharges at the same heating power. Therefore, the Mo burst in the helium discharge is considered to be caused by an enhanced evaporation under the helium irradiation. According to inspection of the in-vessel components after these experiments, severe melting was observed at the edge of the divertor plates. Moreover, at one toroidal location, a liner near the X-point around the divertor coil was also melted. Therefore, these two damages are considered to be the origin of the Mo burst. For example, at the edge of toroidal gaps of the divertor plates, around 10 kW/cm^2 of heat flux is expected. In this condition, the Mo surface temperature reaches 2600°C (its melting point) in 100 to 200 ms. To suppress these Mo burst, the separatrix line was swept on the divertor plate at a speed of 4 cm/sec from t=6 sec to 7 sec as shown in Fig. 20. As a result, the half width of the temperature profile on the divertor plate increased from 2 cm to 4 cm and the temperature rise was decreased by a factor of 2. The above results show that the swing of the separatrix line is effective in reducing the evaporation on the divertor plate.

4. DISCUSSION

(1) NEUTRAL PRESSURE BULD-UP

Nonlinear dependence of the neutral pressure on the main plasma density is explained by the inverse dependence of τ_p on the main plasma density. The neutral pressure in the divertor chamber $P_{H_2}^{DIV}$ is given by $RN_e/(\tau_p C)$, where C is the conductance between the main plasma and the divertor chamber. In this experiment, the conductance is almost constant and recycling ratio R is in the range of 0.87 to 0.99[27]. Therefore, $P_{H_2}^{DIV}$ is proportional to influx to the divertor chamber N_e/τ_p. This gives $\bar{n}_e^2$ dependence of $P_{H_2}^{DIV}$. Moreover, since the compression ratio is almost constant, the neutral pressure around the main plasma, $P_{H_2}^{MAIN}$, also has $\bar{n}_e^2$ dependence. This dependence of $P_{H_2}^{DIV}$ is also obtained in the fluid model divertor simulation [28]. In this simulation, neutral particle density (n_0^{DIV}) was calculated and $\bar{n}_e^2$ dependence of n_0^{DIV} was obtained. Higher neutral particle density in NB heated discharge compared to the OH case was obtained by using reduced τ_p which simulated τ_p degradation during the NB heating phase. Since n_0^{DIV} is proportional to $P_{H_2}^{DIV}$, the experimental results agree qualitatively with the simulation results.

(2) PARTICLE EXHAUST

Saturation characteristics of the pumping rate by the divertor plate can be explained by the saturation fluence of TiC measured in the laboratory experiment [29]. Deposition area is calculated as $4\pi R_p \Delta$, where R_p is the location of the divertor plate from the major axis, and Δ is the effective width of the plasma bombardment. Using R_p = 450 cm and Δ = 5 cm, the deposition area is estimated to be 2.8×10^4 cm^2. With 1.0 s duration of NB injection, the saturation value of 3 Pa m^3/s in Q_{DIV} is equivalent to a fluence of 5.6×10^{16} cm^{-2}. In this experiment, boundary temperature near the divertor plate was not measured. According to the divertor simulation, the electron temperature near the divertor plate is calculated to be around 10 eV for donsities $\bar{n}_e$=5 to 6×10^{19} m^{-3} [28]. Considering sheath potential, incident energy on the divertor plate is in the range of several of tens of eV. According to the laboratory experiment on deuterium retention in TiC, the saturation

value of retained deuterium fluences with of implanted energy 1.5 keV are 1.2×10^{17} cm^{-2} for incident fluence of 10^{18} cm^{-2} [28]. Therefore, considering several tens of eV for the incident energy in this experiment, the average retained fluence is estimated to be around 10^{16} cm^{-2}. This value is almost the same as the fluence calculated for the saturated pumping rate of the divertor plate. However, in a long-pulse discharge (more than 10 s), the pumping rate by the divertor plate is expected to be small because of the full saturation of the divertor plate.

5. SUMMARY

In the 20 MW NB-heated discharges, particle, impurity and heat load are sufficientlly controlled. Major results are summarized as follows:

- Neutral pressures in the divertor chamber and around the main plasma increase in proportion to $\bar{n}_e^2$. The compression rate is about 45.

  In the particle balance, the particle exhaust by the divertor plate is dominant in densities less than 6×10^{19} m^{-3}. On the other hand, in $\bar{n}_e > 6\times10^{19}$ m^{-3}, particle exhaust by the divertor pumping system becomes dominant. Therefore, active pumping system is necessary for particle control in long-pulse NB-heated divertor discharge.

- According to the spatial distribution of the temperature rise on the divertor plate, the half width of heat load is less than 1 cm for $\bar{n}_e$ =1.5 to 4.4×10^{19} m^{-3}.

- The global power balance shows that P_{RAD}^{MAIN}/P_{ABS} is 5% to 10% in the NB-heated divertor discharge, although P_{RAD}^{MAIN}/P_{ABS} in the limiter discharge is 50% to 60%. At $\bar{n}_e=6\times10^{19}$ m^{-3}, $P_{T/C}^{DIV}/P_{ABS}$ is 50% and P_{RAD}^{DIV}/P_{ABS} is 15%.

- The origin of the Mo burst, observed in NB heated helium discharges, is considered to be the edge of the divertor plate or the liner in the divertor throat. Separatrix swing is effective in reducing the

value of retained deuterium fluences with of implanted energy 1.5 keV are 1.2×10^{17} cm^{-2} for incident fluence of 10^{18} cm^{-2} [28]. Therefore, considering several tens of eV for the incident energy in this experiment, the average retained fluence is estimated to be around 10^{16} cm^{-2}. This value is almost the same as the fluence calculated for the saturated pumping rate of the divertor plate. However, in a long-pulse discharge (more than 10 s), the pumping rate by the divertor plate is expected to be small because of the full saturation of the divertor plate.

5. SUMMARY

In the 20 MW NB-heated discharges, particle, impurity and heat load are sufficientlly controlled. Major results are summarized as follows:

- Neutral pressures in the divertor chamber and around the main plasma increase in proportion to $\bar{n}_e^2$. The compression rate is about 45.

  In the particle balance, the particle exhaust by the divertor plate is dominant in densities less than 6×10^{19} m^{-3}. On the other hand, in $\bar{n}_e > 6\times10^{19}$ m^{-3}, particle exhaust by the divertor pumping system becomes dominant. Therefore, active pumping system is necessary for particle control in long-pulse NB-heated divertor discharge.

- According to the spatial distribution of the temperature rise on the divertor plate, the half width of heat load is less than 1 cm for $\bar{n}_e$ =1.5 to 4.4×10^{19} m^{-3}.

- The global power balance shows that P_{RAD}^{MAIN}/P_{ABS} is 5% to 10% in the NB-heated divertor discharge, although P_{RAD}^{MAIN}/P_{ABS} in the limiter discharge is 50% to 60%. At $\bar{n}_e=6\times10^{19}$ m^{-3}, $P_{T/C}^{DIV}/P_{ABS}$ is 50% and P_{RAD}^{DIV}/P_{ABS} is 15%.

- The origin of the Mo burst, observed in NB heated helium discharges, is considered to be the edge of the divertor plate or the liner in the divertor throat. Separatrix swing is effective in reducing the

Mo burst in the NB-heated discharge and useful in alleviating high heat flux problems of the divertor plates, especially in future long pulse tokamaks.

ACKNOWLEDGEMENT

The author would like to acknowledge Drs. Y. Shimomura, M. Nagami and T. Tsuji for their fruitful discussions. They would also like to thank all the members of the JT-60 project who have long dedicated themselves to the construction of the JT-60. We would like to acknowledge Dr. S. Mori for his major role in initiating the JT-60 and Drs. K. Tomabechi and M. Yoshikawa for their continued leadership and support.

Mo burst in the NB-heated discharge and useful in alleviating high heat flux problems of the divertor plates, especially in future long pulse tokamaks.

ACKNOWLEDGEMENT

The author would like to acknowledge Drs. Y. Shimomura, M. Nagami and T. Tsuji for their fruitful discussions. They would also like to thank all the members of the JT-60 project who have long dedicated themselves to the construction of the JT-60. We would like to acknowledge Dr. S. Mori for his major role in initiating the JT-60 and Drs. K. Tomabechi and M. Yoshikawa for their continued leadership and support.

REFERENCES

[1] DIVA GROUP, Nucl. Fusion 18 (1978) 1619.

[2] M. KEILHACKER, G. BECKER, K. BEHRINGER, D. CAMPBELL, A. EBERHAGEN, in Plasma Physics and Controlled Nuclear Fusion Research (Proc. 9th Int. Conf., Baltimore, 1982) Vol. 3, IAEA, Vienna (1983) 183.

[3] Y. SHIMOMURA, M. KEILHACKER, K. LACKNER, H. MURMANN, Nucl. Fusion 23 (1983) 869.

[4] M. SHIMADA, M. WASHIZU, S. SENGOKU, N. SUZUKI, M. NAGAMI, et al., J. Nucl. Mater. 128 & 129 (1984) 340.

[5] R.J. FONCK, M. BELL, K. BOL, R. BUDNY, P. COUTURE, et al., J. Nucl. Mater. 128 & 129 (1984) 330.

[6] F. WAGNER, G. BECKER, K. BEHRINGER, D. CAMPBELL, A. EBERHAGEN, et al., Phys. Rev. Letter. 49 (1982) 1408.

[7] M. MAENO, K. IOKI, S. IZUMI, A. KITSUNEZAKI, M. NAGAMI, et al., Nucl. Fusion 21 (1981) 1474.

[8] M. SHIMADA, M. NAGAMI, K. IOKI, S. ISUMI, M. MAENO, et al., Phys. Rev. Lett. 47 (1981) 350 and Nucl. Fusion 22 (1982) 643.

[9] M.A. MAHDAVI, J.C. DeBOO, C.L. HSIEH, N. OHYABU, R.D. STAMBAUGH, et al., Phys. Rev. Lett. 47 (1981) 1602.

[10] K. ODAJIMA, A. FUNAHASHI, K. HOSHINO, S. KASAI, T. KAWAKAMI, et al., in Plasma Physics and Controled Nuclear Fusion Research (Proc. 11th Int. Conf., Kyoto, 1986) IAEA-CN-47/A-III-2, to be published.

[11] J. LUXON, P. ANDERSON, F. BAITY, C. BAXI, G. BRAMSON, et al., ibid, IAEA-CN-47/A-III-3, to be published.

[12] A. TANGA, M. KEILHACKER, D. BARLETT, K. BEHRINGER, R.J. BICKERTON, et al., ibid, IAEA-CN-47/K-I-1, to be published.

[13] M. YOSHIKAWA, K. TOMABECHI, Nucl. Technology/Fusion 4 (1983) 299.

[14] Y. SHIMOMURA, K. SHIMIZU, T. HIRAYAMA, M. ASUMI, H. NINOMIYA, J. Nucl. Mater. 128 & 129 (1984) 19.

[15] JT-60 TEAM (presented by M. YOSHIKAWA), Plasma Physics and Controlled Fusion 28 (1986) 165.

[16] JT-60 TEAM (presented by S. TAMURA), Plasma Physics and Controlled Fusion 28 (1986) 1377.

[17] JT-60 TEAM (presented by H. KISHIMOTO), J. Nucl. Mater. 145 & 147 (1987) 41.

[18] M. YOSHIKAWA, T. ABE, H. AKAOKA, H. AIKAWA, H. AKASAKA, et al., in Plasma Physics and Controlled Nuclear Fusion Research (Proc. 11th Int. Conf., Kyoto, 1986, IAEA-CN-47/A-I-1) to be published.

[19] JT-60 TEAM (presented by M. NAGAMI), ibid, (IAEA-CN-47/A-II-2).

[20] JT-60 TEAM (presented by H. TAKEUCHI), ibid, (IAEA-Cn-47/A-IV-3).

[21] M. OHTA, T. ABE, N. AKINO, T. ANDO, T. ARAI et al., Fusion Engrg. Des. 5 (1987) 27.

[22] H. NAKAMURA, T. ANDO, M. MASUDA, M. SHIMIZU, T. SHIMIZU, et al., Proc. 10th Symp. on Fusion Engineering, Philadelphia, Dec. 1983, Vol. 2, 1022.

[23] Y. MURAKAMI, T. ABE, H. NAKAMURA, J. Nucl. Mater. 111 & 112 (1982) 861.

[24] T. ANDO, H. NAKAMURA, H. YOSHIDA, H. SUNAOSHI, T. ARAI, et al., Proc. 14th Symp. on Fusion Technology, Avignon, Sept. 1986.

[25] H.F. DYLLA, M.G. BELL, R.J. FONCK, K. JAEHNIG, S.M. KAYE, et al., J. Nucl. Mater. 121 (1984) 144.

[26] S. TSUJI and JT-60 Team, in Controlled Fusion and Plasma Physics (Proc. 14th Europ. Conf., Madrid, 1987), Vol. 2 (1987) 57.

[27] K. YAMADA, S. TSUJI, K. SHIMIZU, T. NISHITANI, K. NAGASHIMA, "A study of the Particle Confinement Properties in Ohmically and Neutral Beam Heated Plasmas of the JT-60 Tokamak", to be published in Nucl. Fusion.

[28] H. YOSHIDA, S. NIIKURA, K. SHIMIZU, T. ANDO, H. NAKAMURA, et al., "Divertor Analysis for the Ohmically and Neutral Beam Heated Discharges in JT-60 (Letter)", submitted to Nucl. Fusion.

[29] B.L. DOYLE, D.K. WAMPLER, D.K. BRICE, S.T. PICRAUX, J. Nucl. Mater. 93&94 (1980) 551.

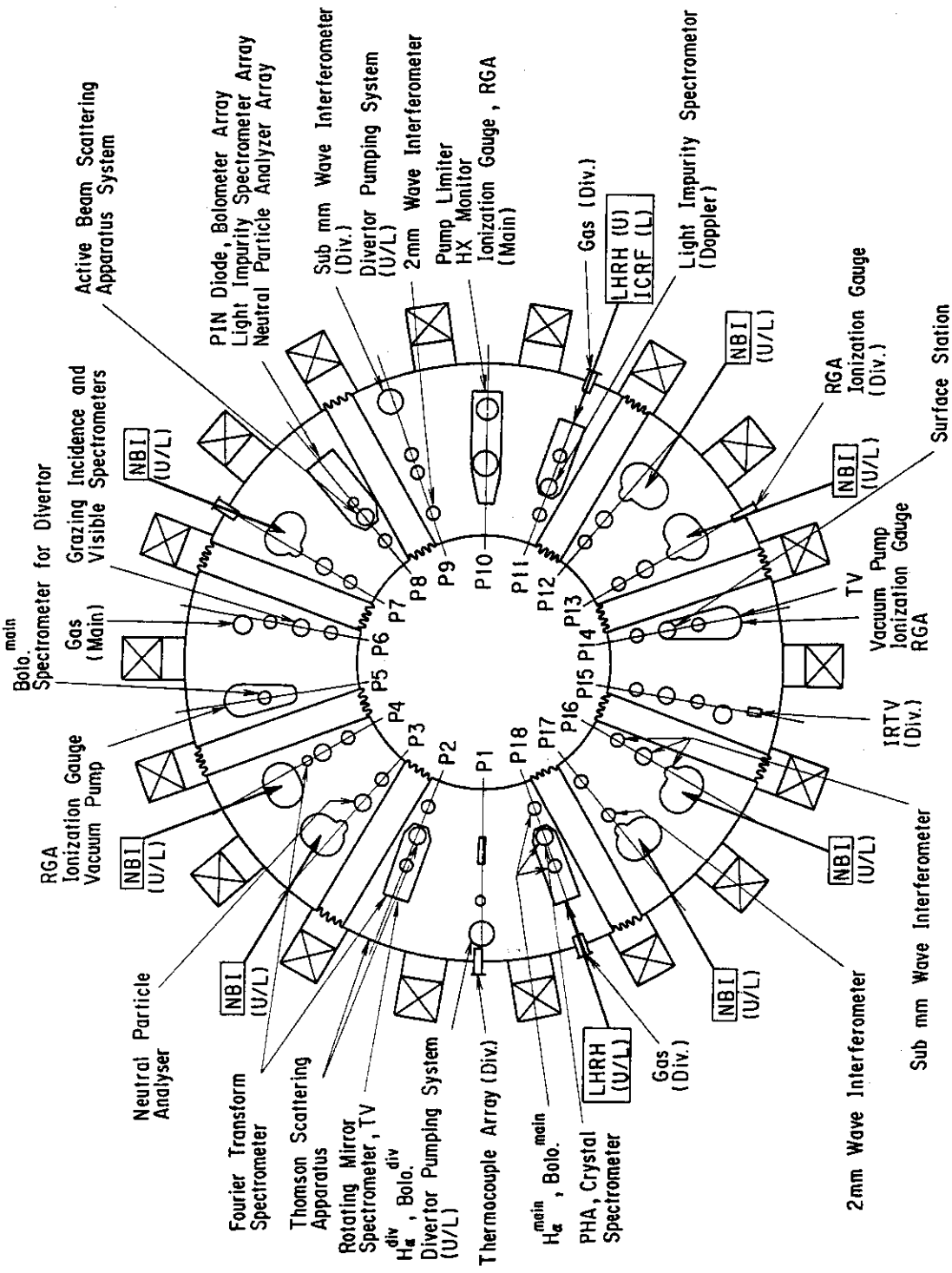

Fig. 1 Schematic top view of JT-60 showing the location of diagnostics and major components.

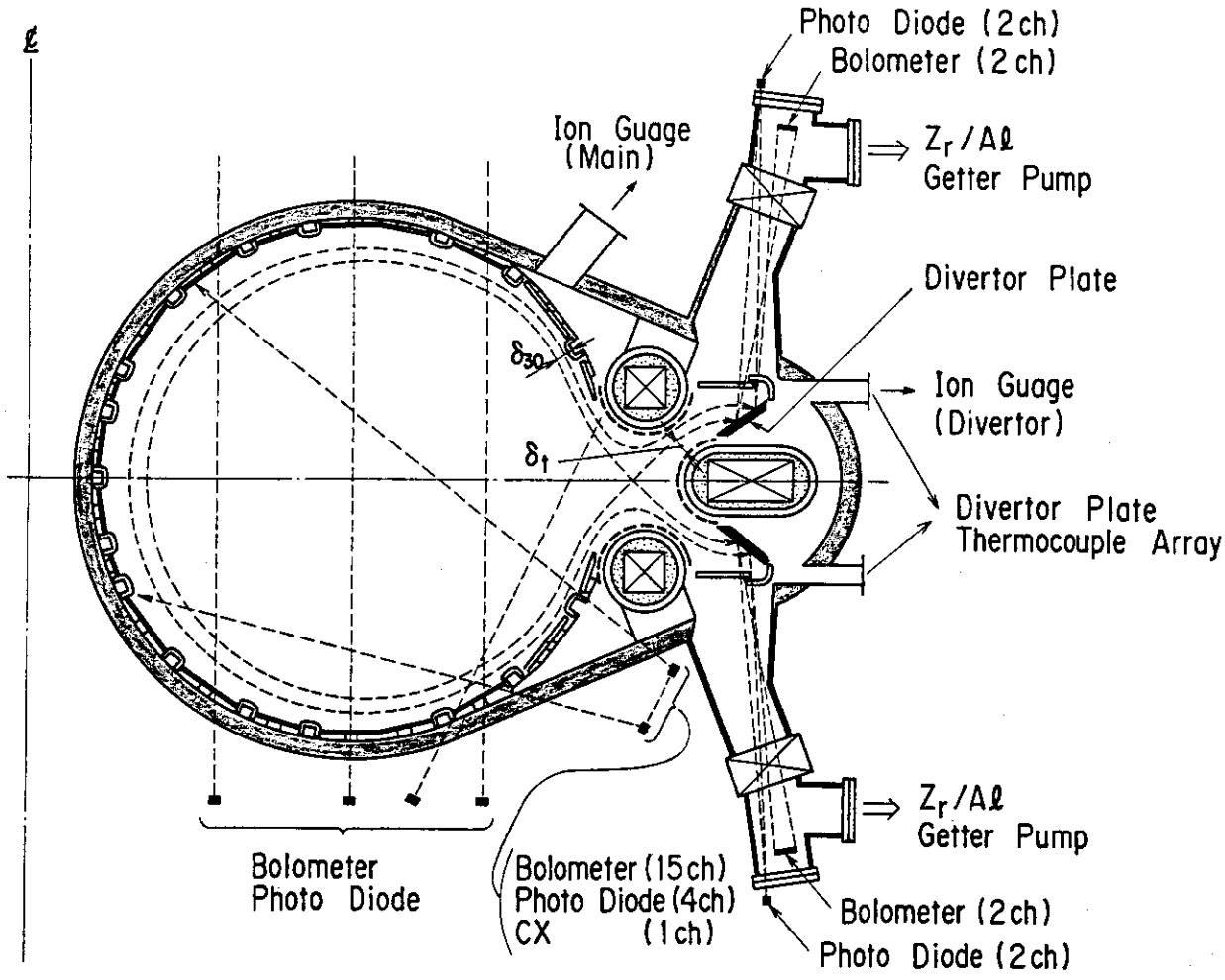

Fig. 2 Cross sectional view of JT-60 showing divertor diagnostics and divertor pumping port.

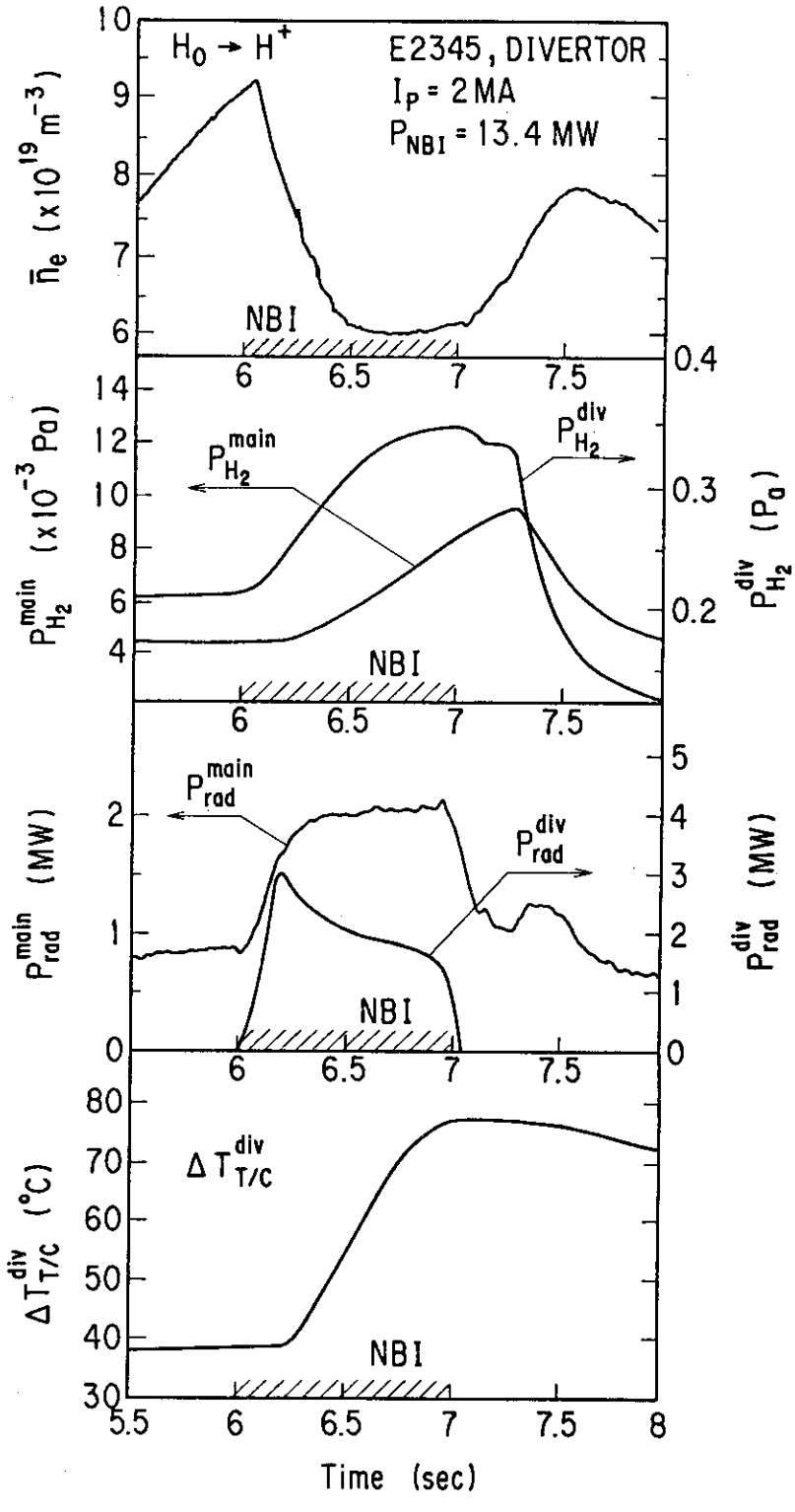

Fig. 3 Time evolution of main plasma density ($\bar{n}_e$), neutral pressures in divertor chamber ($P_{H_2}^{DIV}$) and around the main plasma ($P_{H_2}^{MAIN}$), radiation loss in the main (P_{RAD}^{MAIN}) and divertor plasmas (P_{RAD}^{DIV}), temperature rise in the divertor plate ($\Delta T_{T/C}^{DIV}$) for 2-MA hydrogen discharge with 13.4-MW NB heating.

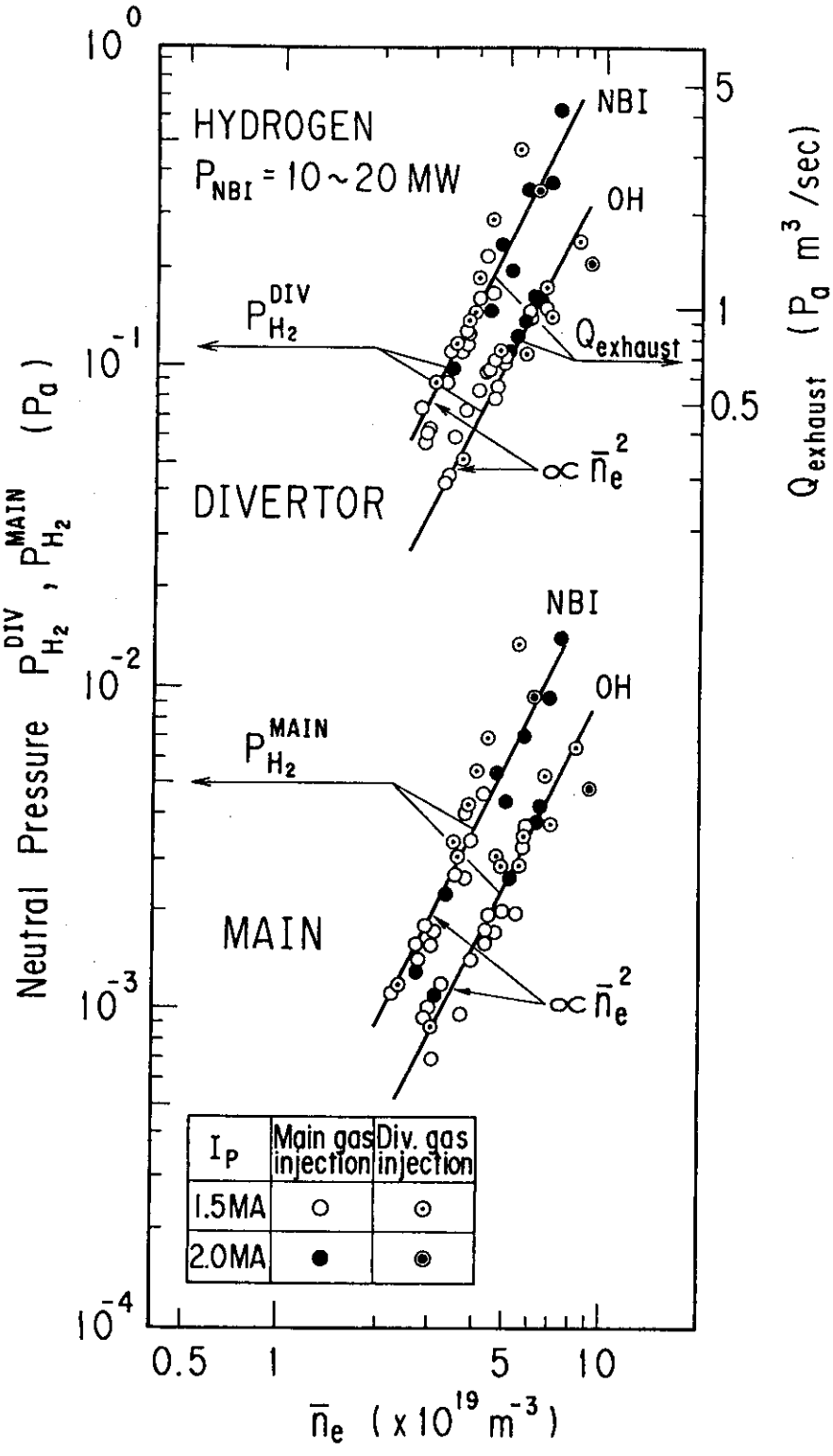

Fig. 4 Density dependences of neutral pressures in the divertor chamber ($P_{H_2}^{DIV}$) and around the main plasma ($P_{H_2}^{MAIN}$) for ohmically-heated and NB-heated discharges. Particle exhaust rate ($Q_{exhaust}$) can be derived from the $P_{H_2}^{DIV}$ data ($Q_{exhaust}$ = 6.8 $P_{H_2}^{DIV}$).

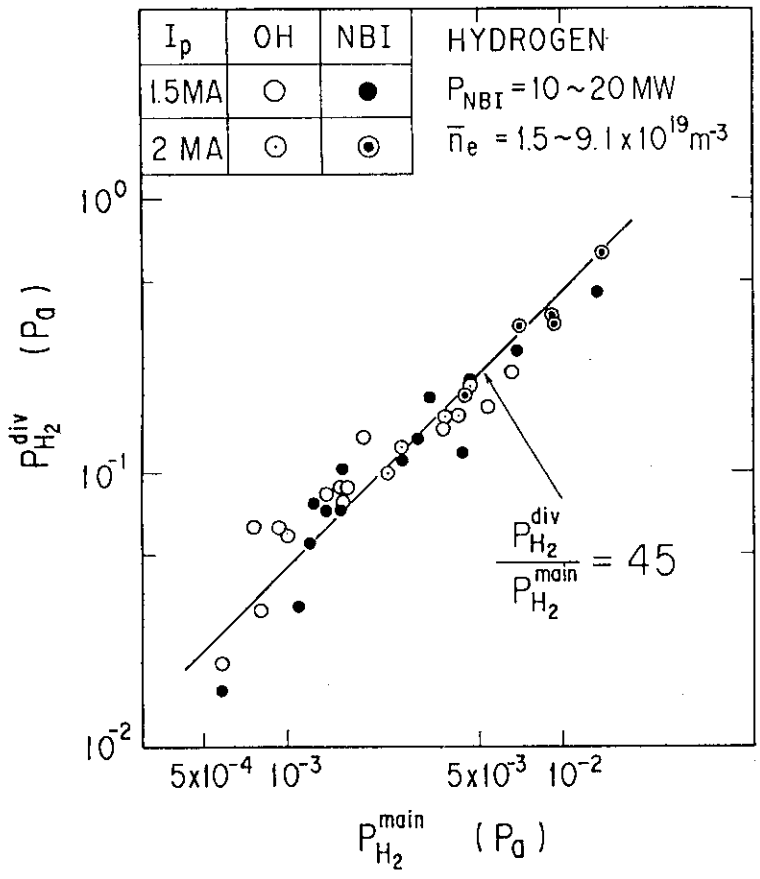

Fig. 5 Relation between the neutral pressures in the divertor chamber and around the main plasma.

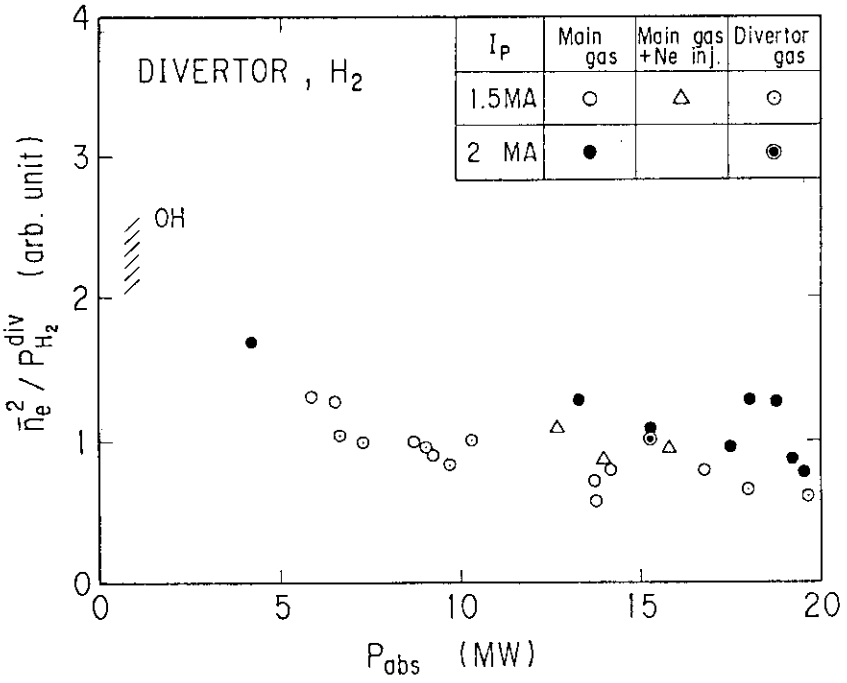

Fig. 6 Dependence of characteristic parameter ($\bar{n}_e^2/P_{H_2}^{DIV}$) on the absorbed NB power. This parameter is in proportion to the particle confinement time τ_p.

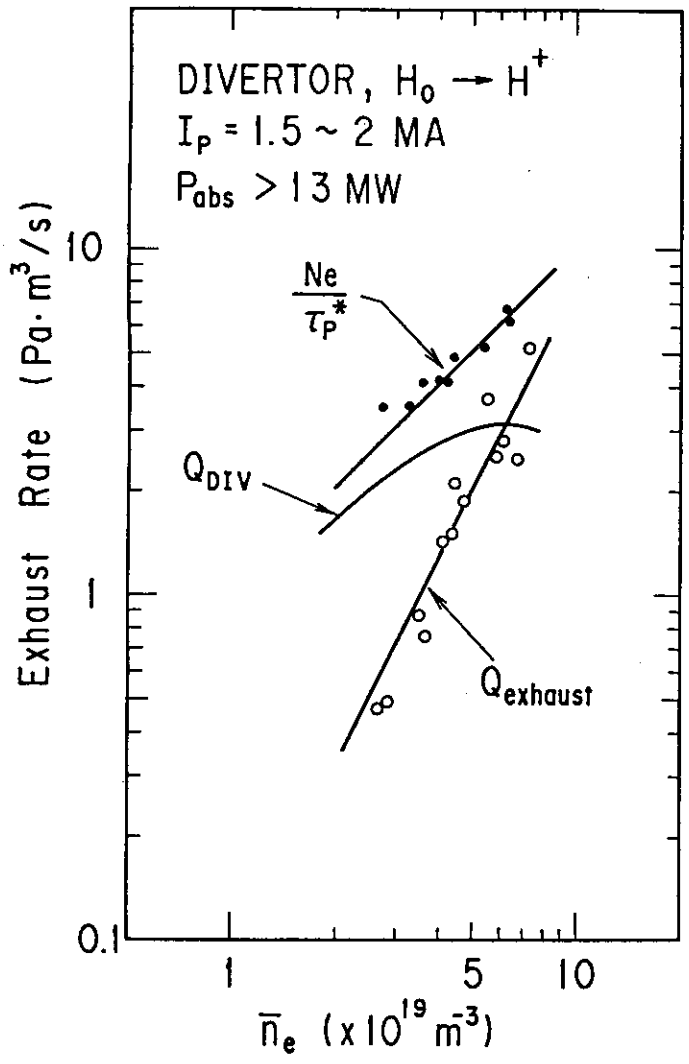

Fig. 7 Density dependence of total exhaust rate (N_e/τ_p^*) and pumping rate by the divertor plate (Q_{DIV}) and the divertor pumping system ($Q_{exhaust}$).

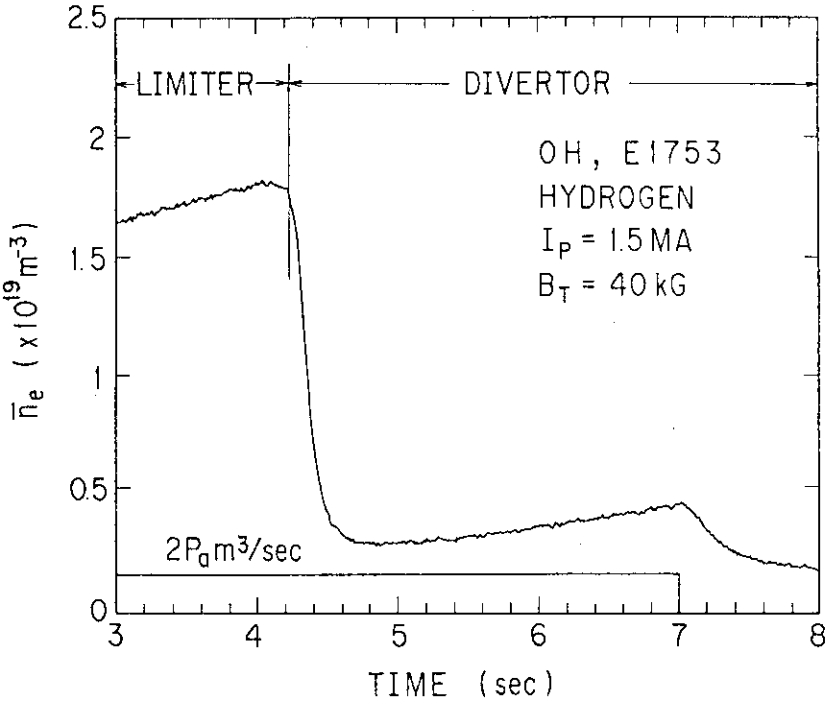

Fig. 8 Time evolution of main plasma density in limiter-divertor transition experiment.

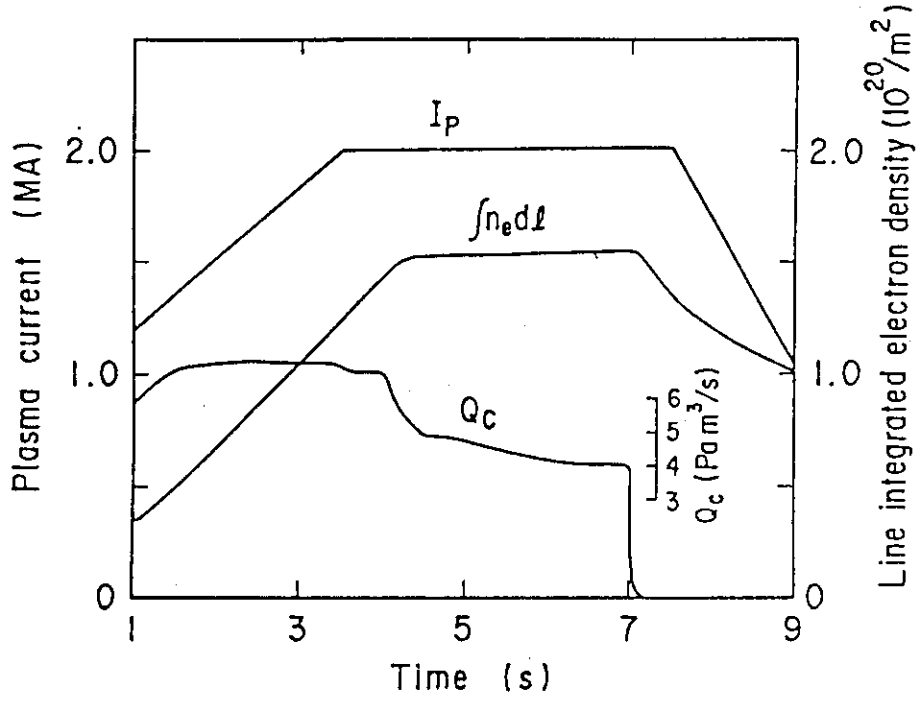

Fig. 9 Time evolution of main plasma density, plasma current and gas injection rate in density feed-back control experiment.

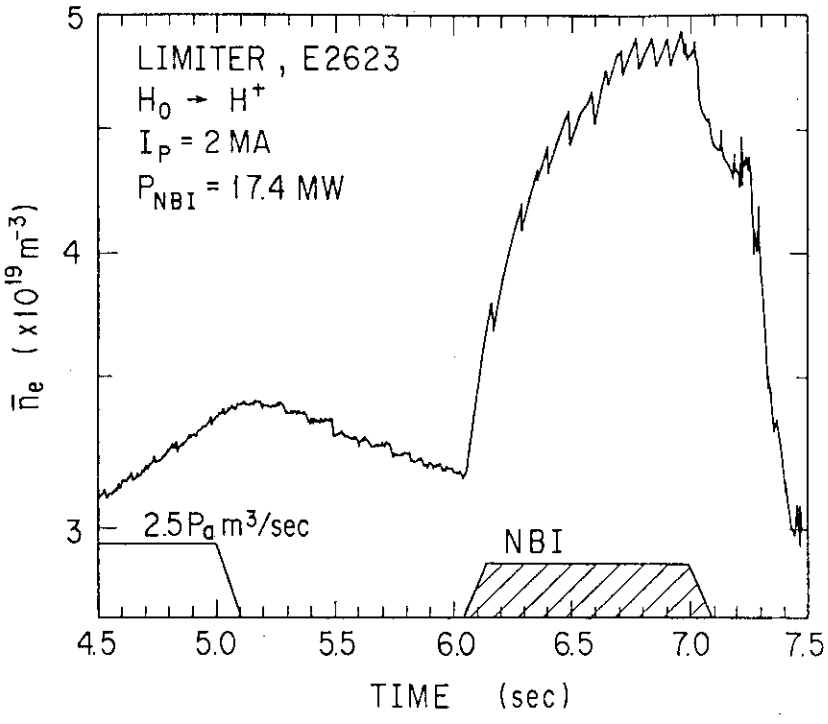

Fig. 10 Time evolution of main plasma density in the NB-heated limiter discharge.

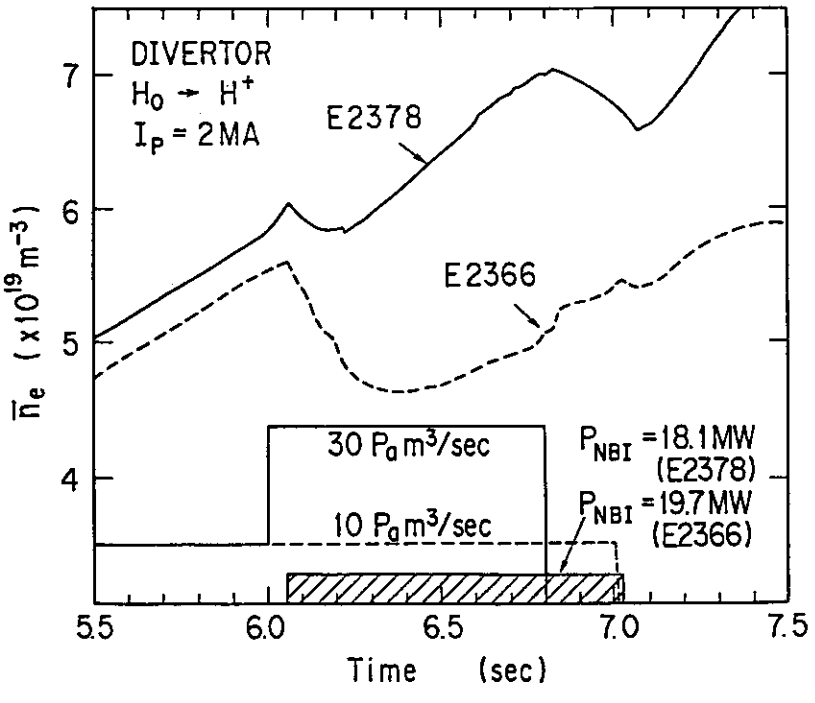

Fig. 11 Time evolution of main plasma density in the NB-heated divertor discharge, showing density control by gas gas puffing.

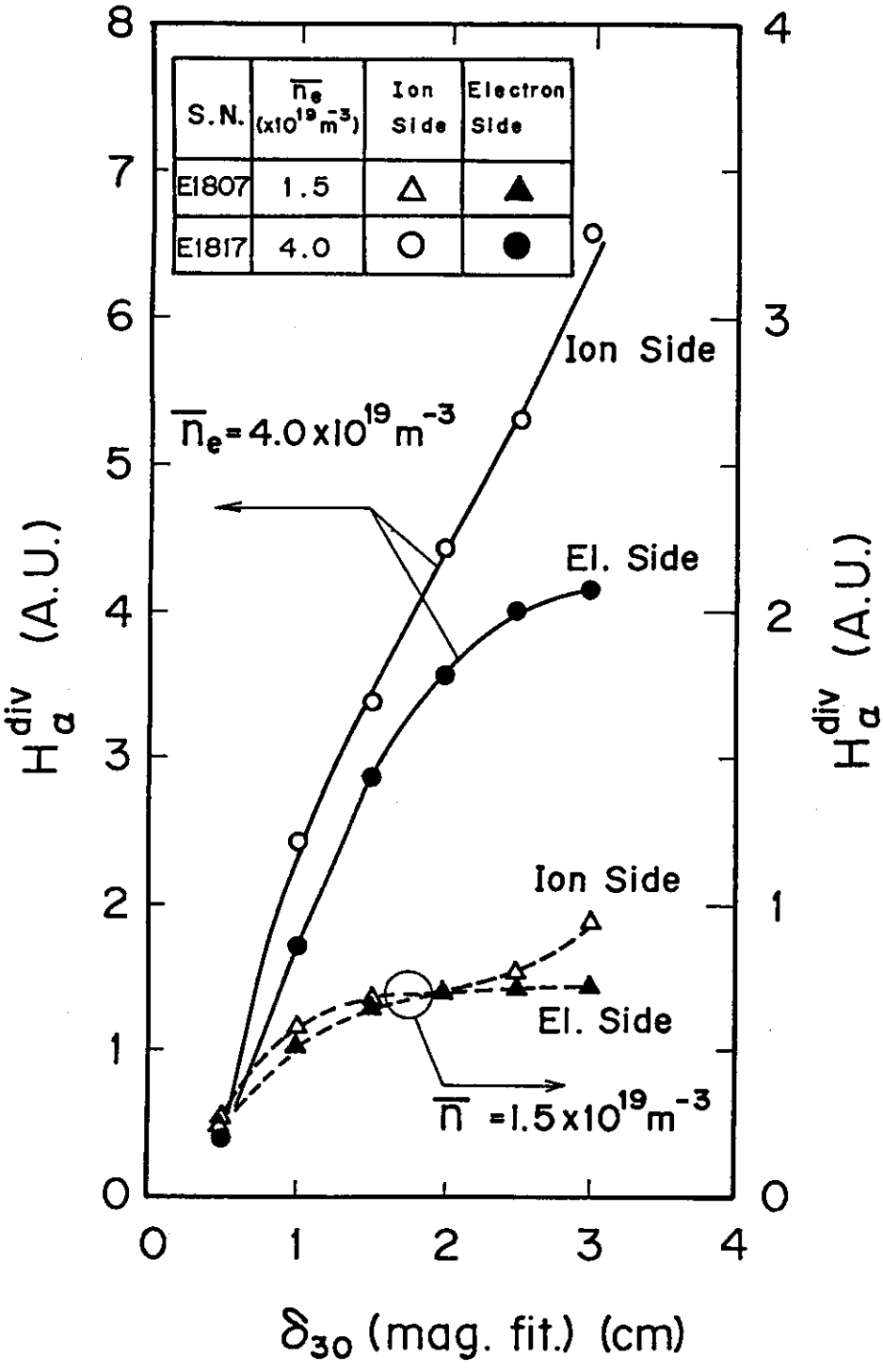

Fig. 12 Dependence of divertor H_α on the clearance between the separatrix magnetic surface and the fixed limiter in the clearance scanning experiment.

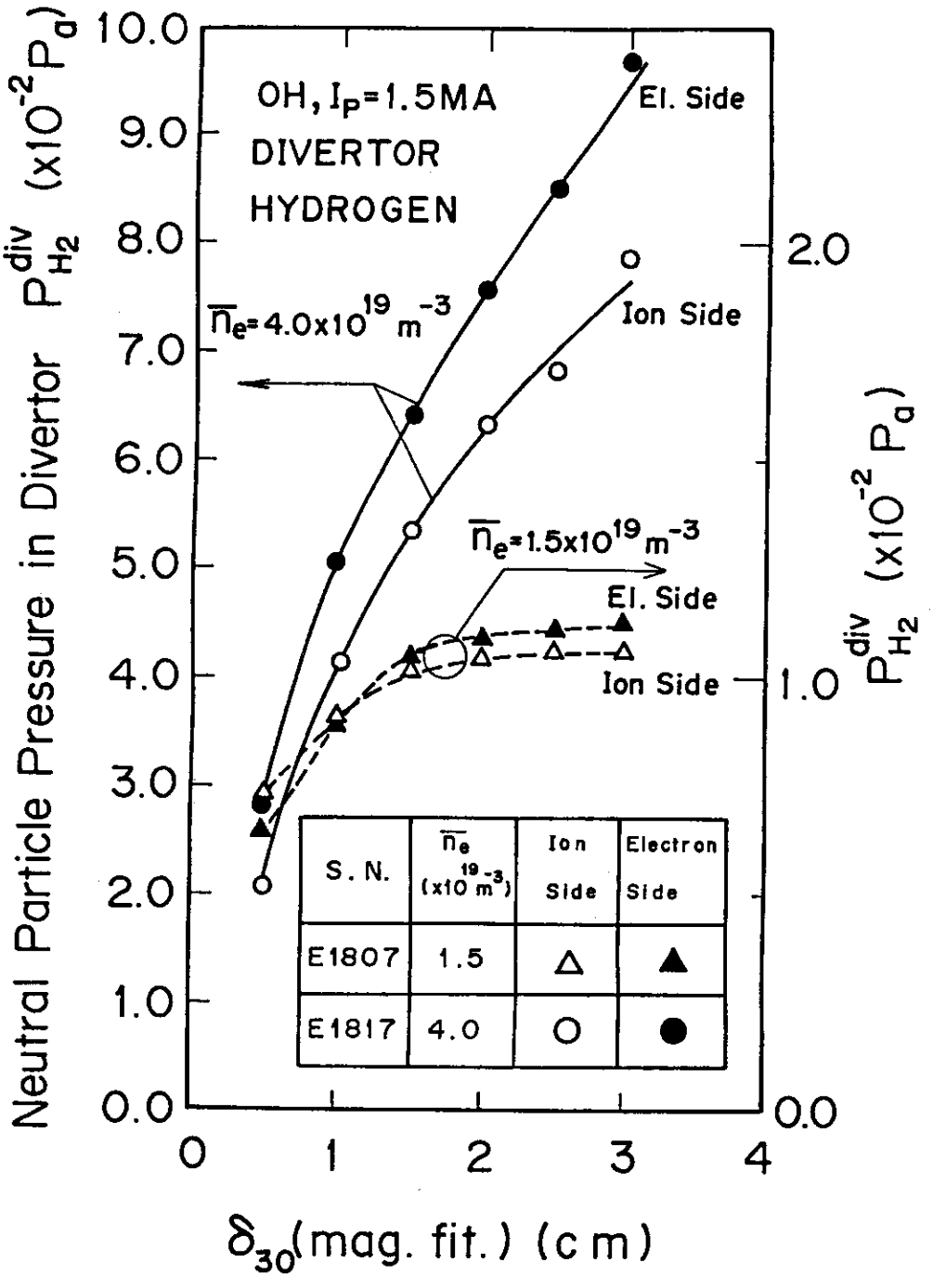

Fig. 13 Dependence of divertor neutral pressure on the clearance between the separatrix magnetic surface and the fixed limiter in the clearance scanning experiment.

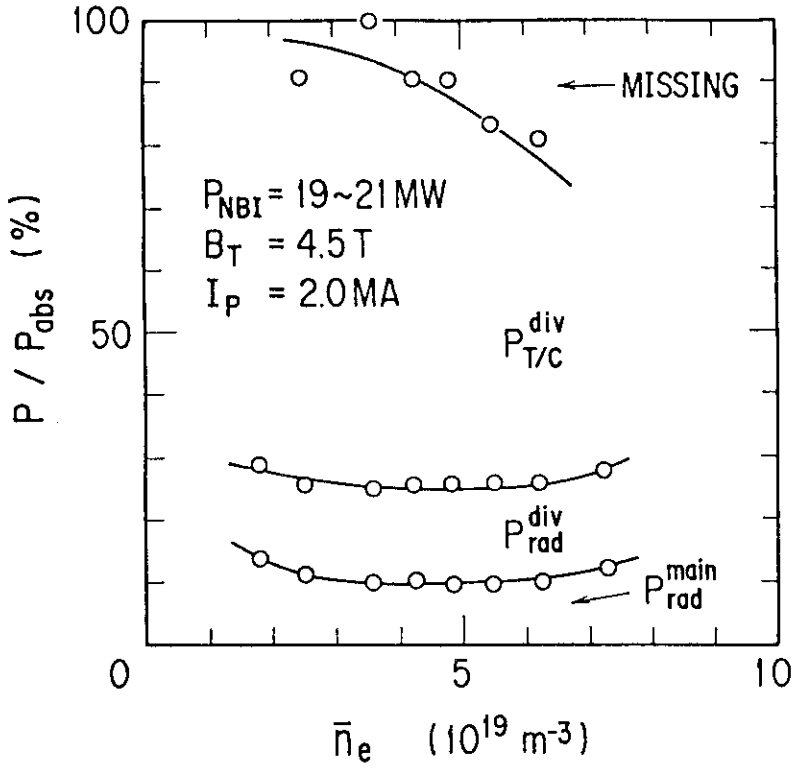

Fig. 14 Global power balance for NB-heated hydrogen discharge. Fractional heat load power to absorbed NB power is plotted. Main causes of the missing power are radiation losses from the X-point and the divertor chamber near the X-point.

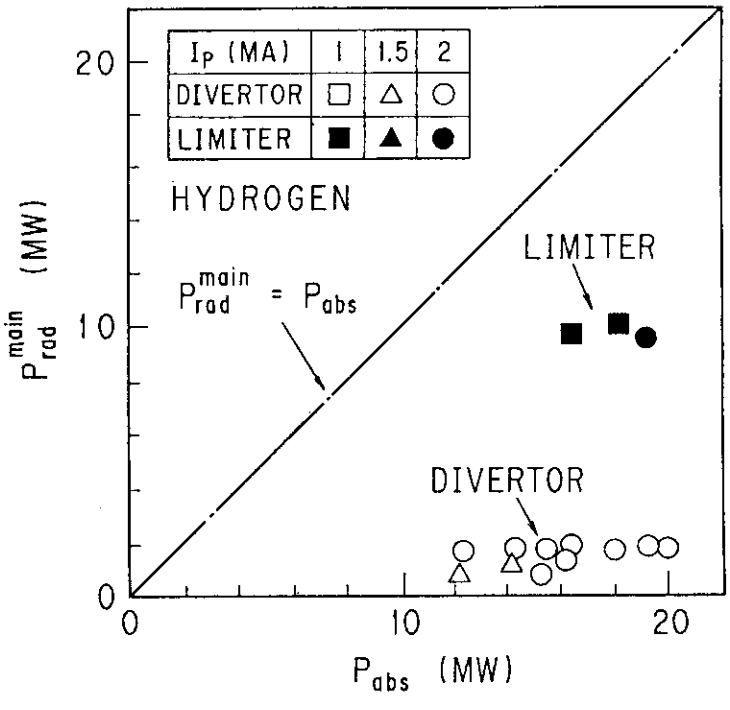

Fig. 15 Ratios of main plasma radiation losses to absorbed power in the NB-heated limiter and divertor discharges.

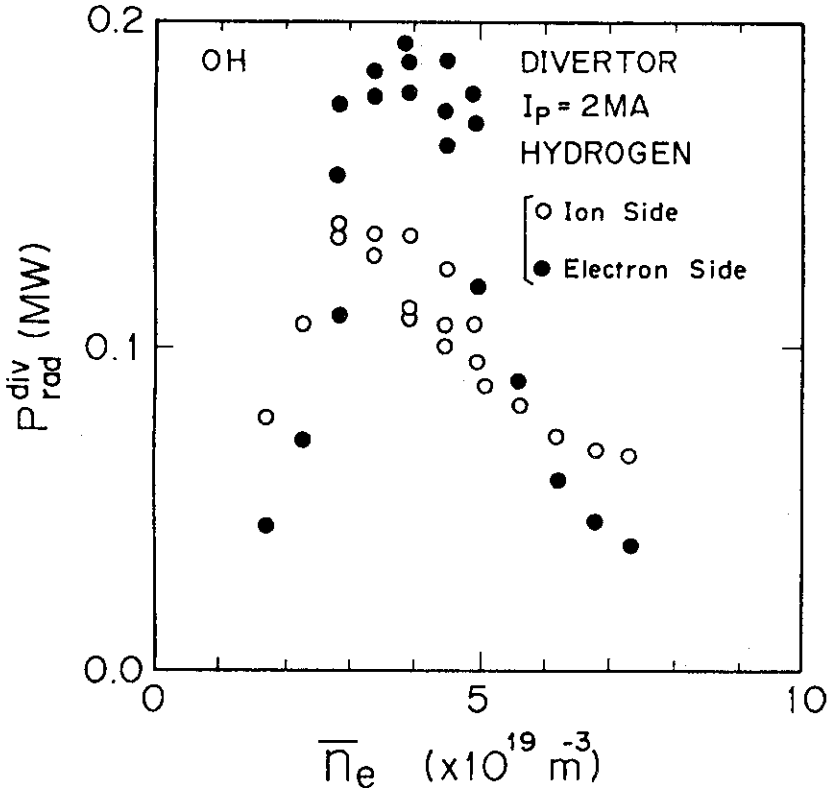

Fig. 16 Density dependence of divertor radiation loss in ohmically heated discharges.

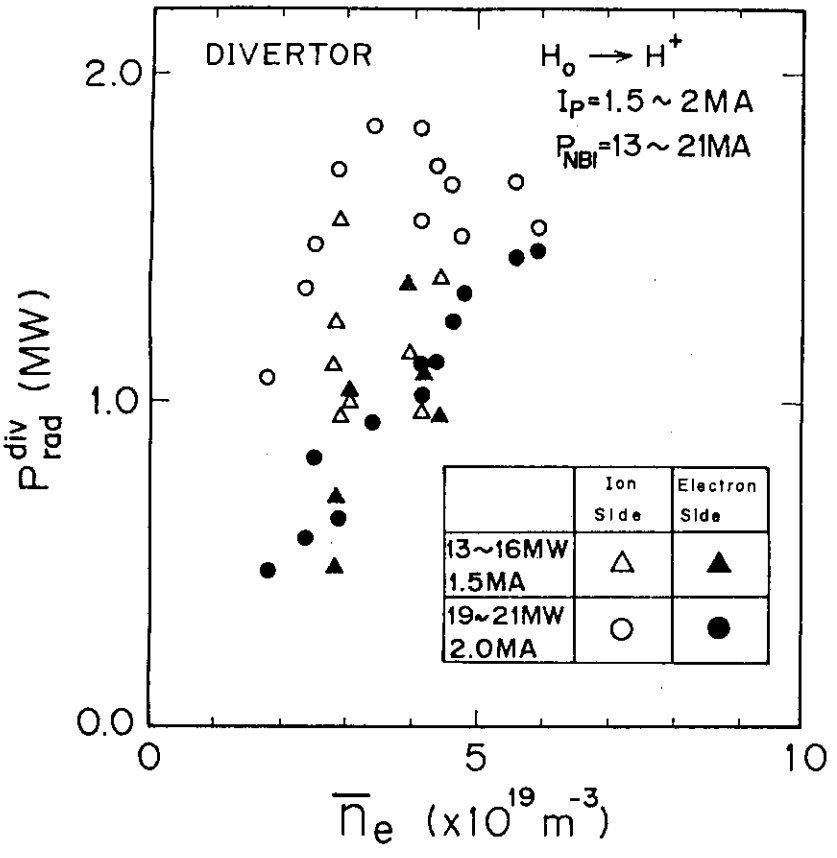

Fig. 17 Density dependence of divertor radiation loss in NB-heated discharges.

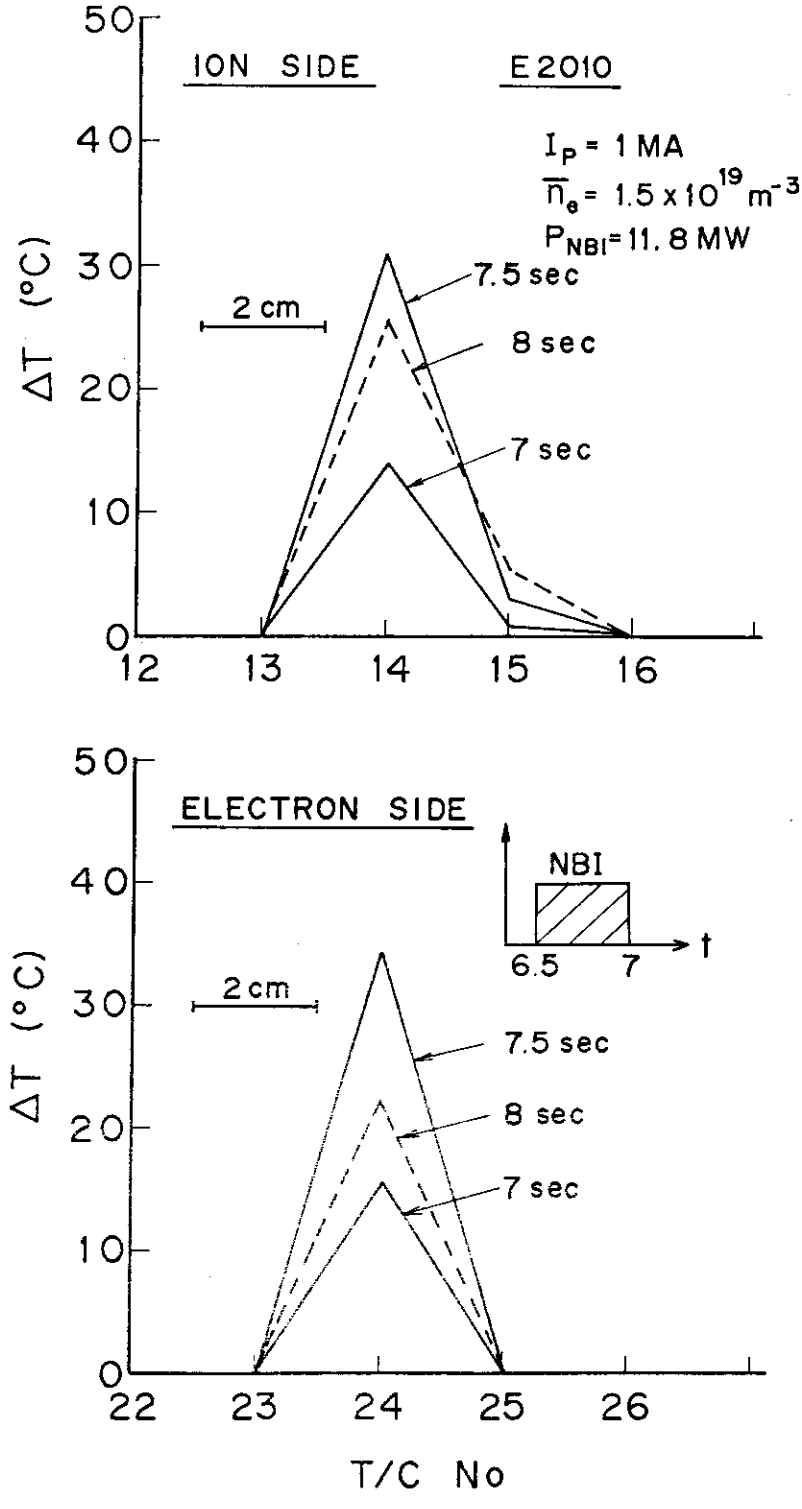

Fig. 18 Spatial distribution of temperature rises of brazed thermocouples in the divertor discharge with $\bar{n}_e$=1.5×10^{19} m^{-3}.

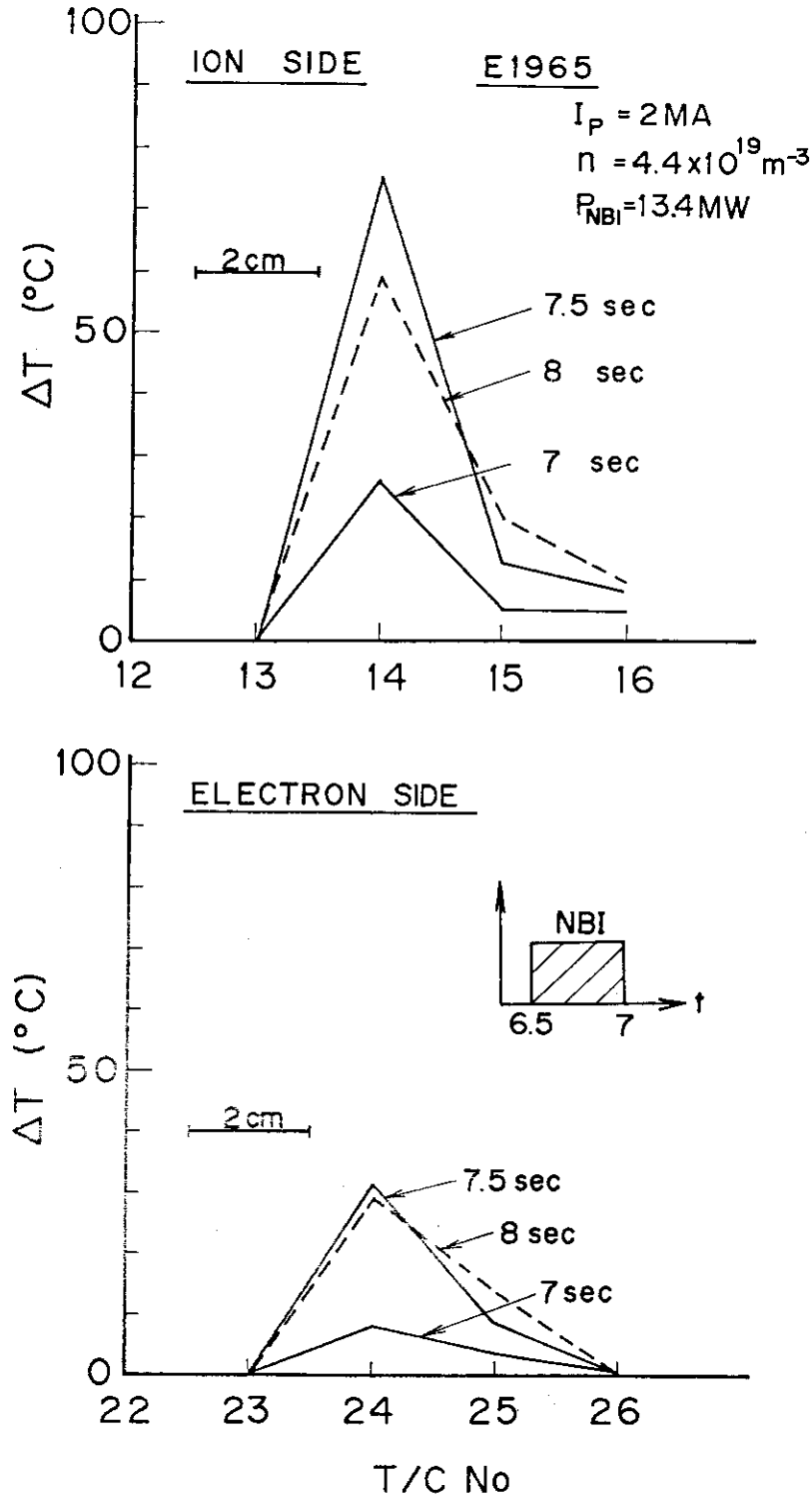

Fig. 19 Spatial distribution of temperature rises of brazed thermocouples in the divertor discharge with $\bar{n}_e$=4.4×10^{19} m^{-3}.

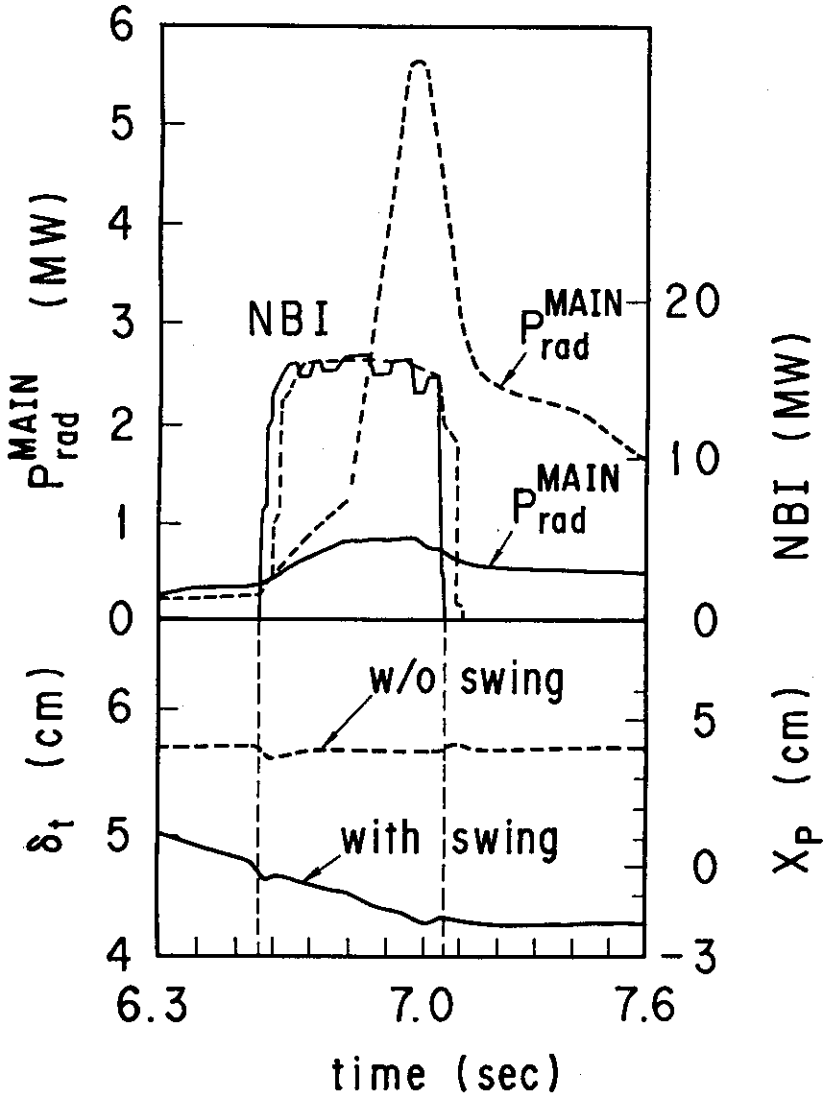

Fig. 20 Time evolution of main plasma radiation losses in the NB-heated divertor helium discharges with and without separatrix swing.